SAND99-1211J

Large Friction Anisotropy of a Polydiacetylene Monolayer

running title: "Friction Anisotropy of Polydiacetylene"

R.W. Carpick[1], D.Y. Sasaki[2], and A.R. Burns[1,3]

[1] *Sandia National Laboratories, Surface and Interface Sciences, Albuquerque, NM 87185-1413.*

[2] *Sandia National Laboratories, Organic Materials Aging and Reliability, Albuquerque, NM 87185-1407.*

[3] *Corresponding author. E-mail: aburns@sandia.gov, tel: 505-844-9642, fax: 505-844-5470*

Abstract

Friction force microscopy measurements of a polydiacetylene monolayer film reveal a 300% friction anisotropy that is correlated with the film structure. The film consists of a monolayer of the red form of N-(2-ethanol)-10,12 pentacosadiynamide, prepared on a Langmuir trough and deposited on a mica substrate. As confirmed by atomic force microscopy and fluorescence microscopy, the monolayer consists of domains of linearly oriented conjugated backbones with pendant hydrocarbon side chains above and below the backbones. Maximum friction occurs when the sliding direction is perpendicular to the backbone. We propose that the backbones impose anisotropic packing of the hydrocarbon side chains which leads to the observed friction anisotropy. Friction anisotropy is therefore a sensitive, optically-independent indicator of polymer backbone direction and monolayer structural properties.

Keywords: atomic force microscopy, friction force microscopy, friction anisotropy, friction asymmetry, nanotribology, polydiacetylene, LB films, directional dependence, fluorescence

1. Introduction

Recent fundamental studies of friction at the atomic or molecular level have revealed behavior distinct from common macroscopic experience [1], such as violation of Amonton's Law [2], adhesion hysteresis [3], and dependence upon sliding velocity [4] and direction [5-13]. The dependence of friction upon sliding direction arises from structural properties of the materials in contact. As such, friction measurements can reveal specific structural properties, such as molecular or crystallographic orientation, which may not be seen in topographic images. Such experiments can then elucidate how friction is fundamentally related to these structural properties. Furthermore, anisotropic friction forces can be exploited for the purpose of nanofabrication [9] by providing preferred pathways for interfacial sliding of nanocomponents.

Friction anisotropy refers to the variation of friction with the relative orientation angle between sliding surfaces, or with the sliding direction itself. For example, Hirano and Shinjo [5] observed frictional anisotropy between bare mica surfaces in a surface forces apparatus. In one experiment, they fixed the sliding direction and varied the relative orientation of the crystallographic axes (the misfit angle) of the opposing surfaces, observing maximum friction when the axes were aligned (commensurate). In another experiment, they fixed the crystal axes in the aligned orientation while the sliding direction was varied, observing lowest friction when the sliding direction coincided with the primitive vectors of the surfaces. Using the atomic force microscope (AFM), Sheehan and Lieber [9] demonstrated that MoO_3 islands on a MoS_2 substrate could be displaced by the AFM tip, but only along preferred directions that were determined by the given alignment of the MoO_3 and MoS_2 crystal axes. In these two cases, friction anisotropy was correlated with the relative crystallographic orientation of the sliding interface. Friction anisotropy has also been observed between AFM tips and surfaces with molecular groups tilted with respect the surface normal, such as ferroelectric materials [7,8] and lipid monolayers [11].

In addition, these groups also observed *friction asymmetry*, which refers to a change in friction when the sliding direction is changed by 180° (*i.e.* from back to forth).

In this study, we examine friction anisotropy of a polydiacetylene monolayer film, polymerized from the monomer N-(2-ethanol)-10,12 pentacosadiynamide (PCEA). In general, ordered diacetylene molecular layers can be formed by Langmuir-Blodgett (LB) techniques [14,15] or self-assembly [16-18]. The molecular film consists of pendant methylene side chains attached to either side of a polymerized diacetylene backbone that is oriented parallel to the substrate. A PCEA monolayer is illustrated in Fig.1. Polydiacetylenes are an important class of organic materials as they exhibit strong optical absorption that is altered by thermal annealing [19,20], mechanical stress [21-23], or chemical and biological attachment [24-26]. These transitions are correlated with changes in molecular conformation that are not fully understood [14]. Recently we have observed a mechanically-induced color transition in polydiacetylene at the nanometer-scale using scanning probe microscopy [27].

2. Experimental

Details of our sample preparation will be described elsewhere [27,28]. Briefly, the diacetylene amphiphile N-(2-ethanol)-10,12-pentacosadiynamide (PCEA) was prepared by coupling ethanolamine with 10,12-pentacosadiynoyl chloride in tetrahydrofuran and triethylamine. The acid chloride was prepared from 10,12-pentacosadiynoic acid (Farchan/GFS Chemicals, Powell, OH) using oxalyl chloride in methylene chloride. PCEA was isolated by flash column chromatography on silica gel (25% ethylacetate/hexanes, $R_f = 0.23$). Although the product was pure white immediately after isolation, upon standing in the freezer for a day the crystals became tinted with a blue color.

Langmuir monolayers of the PCEA amphiphile were prepared and polymerized by UV light on the water surface. The circular Langmuir trough (Nima, Coventry, UK) was situated on a

vibration isolated table inside a class 100 clean room. The subphase used was deionized water with a resistivity of >18 MΩ-cm (Barnstead Nanopure system, Dubuque, IA) kept at a temperature of 15 ± 0.2 °C. Freshly cleaved muscovite mica were situated horizontally 1 – 2 mm below the water surface prior to monolayer spreading. A 50% chloroform/benzene solution of PCEA was prepared and run through a 0.2 micron filter to remove small traces of red polymer in solution prior to deposition on the water surface. The monolayer was compressed at a rate of 100 cm^2/min to a pressure of 20 mN/m, corresponding to a molecular area of ca. 20 $Å^2$/molecule. Unlike 10,12-pentacosadiynoic acid films, which form trilayers under identical conditions, the PCEA formed a stable monolayer with a collapse pressure of ca. 35 mN/m. All films were equilibrated for 20 – 30 min. at 20 mN/m, prior to UV light exposure (254 nm) with a pair of Hg pen lamps (Oriel, Stratford, CT) spaced 8 cm apart. The lamps were situated 10 cm above the monolayer and the exposure time was 30 seconds. The polymerized monolayer was deposited on the underlying mica by slowly lowering the water level in the trough by aspirating water away. The mica substrate was then taken out of the trough using forceps and allowed to dry in clean room air and then stored in a dark, nitrogen-purged container. Figure 1 shows the proper orientation of the monolayer to the mica substrate with the hydrophilic head group oriented to the interface and the hydrophobic tails pointed away.

Microscopic sample fluorescence was recorded using a Leitz optical fluorescence microscope equipped with dichroic beam filters and polarized white light from a Xenon lamp. A CCD camera was used to capture the field of view for the images presented here. A Nanoscope IIIA atomic force microscope (AFM) (Digital Instruments, Santa Barbara, CA) operating in contact mode was used to obtain topographic and friction force images. Measurements with the AFM were acquired under laboratory ambient conditions. The scan rate was 3 Hz (= lines/sec) unless otherwise noted. A single silicon nitride cantilever (Digital Instruments, Santa Barbara, CA) with a nominal normal force constant of 0.06 N/m was used for all measurements. Friction

measurements were obtained in conventional fashion by scanning the cantilever perpendicular to its long axis at constant load while recording lateral-force induced twisting, and then calculating the difference between 'trace' and 'retrace' scans ('friction loop width'). Because of the inherent difficulty in calibrating the lateral force response of AFM cantilevers [29], lateral forces are reported in raw units (signal Volts).

It is crucial to ensure that the AFM probe tip is not geometrically anisotropic, otherwise tip-induced friction anisotropy may result, providing misleading results. To characterize the tip geometry, we used 'inverse imaging' [2,29] by scanning the tip at the lowest possible load over a substrate consisting of a microfabricated array of silicon tips with a <10 nm curvature radius (NT-MDT, Moscow, Russia). The high resolution contact mode image then represents a convolution of this small feature with the AFM tip. Since the AFM tip has significantly larger curvature than 10 nm, the observed profile is dominated by features of the AFM tip. Several members of the nanotip array are compared to verify that the observed profile is reproducible and not affected by anomalous features of a particular nanotip. We emphasize that the *majority* of AFM tips we characterized possessed anisotropic shapes, double tips and other unsuitable structures. The AFM tip selected for this study consisted of a single, symmetric protrusion within the measurement error. Specifically, we measured orthogonal cross-sections of the last 2 nm of the tip, giving effective curvature radii of 27±3 nm and 32±4 nm. While it is possible that this method may not uncover small anisotropic AFM tip features at the atomic scale, this method allows us to avoid grossly anisotropic tips. To our knowledge, this is the only study of friction anisotropy where the AFM probe tip was characterized in this fashion.

3. Results

3.1 Polarized Fluorescence Microscopy

Polarized fluorescence microscopy reveals that the PCEA film is strongly fluorescent and organized into crystalline domains (Fig. 2). The domains range in size from 10-100 μm and possess irregularly-shaped boundaries. Furthermore, the film coverage is nearly complete, indicating that a high quality film is produced on the trough, and is not seriously disrupted by the transfer process. The fluorescence intensity of each domain varies as the incident polarization angle is changed, and can be almost completely extinguished. Both the absorption and emission dipole of polydiacetylene is known to be aligned along the backbone direction [30-32]. Thus, the polymer backbones are highly oriented within individual domains. Fluorescence intensity variations within the domains are observed in the form of linear striations. The direction of these striations coincides with the polarization angle that produces maximum fluorescence. Therefore, the striations reveal the backbone direction within each domain. The striations may be produced by variations of the film density, which will be discussed further below.

3.2 Friction Anisotropy

AFM images (Fig. 3) reveal film structure that is consistent with the fluorescence microscopy. The 50×50 μm^2 friction image reveals the individual domains, as the friction force varies substantially from one domain to the next, and is nearly uniform within each domain. The topographic image reveals a flat film with some material, 2-4 nm high, situated at a significant fraction of the domain boundaries. Occasionally a small crack in the film revealing the mica substrate is found. This allows measurement of the film height, which we observe to be 2.3±0.3 nm, corresponding to a monolayer with an average tilt of ~30°. Topographic and friction images (500×500 nm^2) within a single domain reveal parallel striations of varying width and uniform direction (Fig. 4), similar to previous reports[33,20]. The total height variation between these striations is ~2 Å. These striations are clearly associated with the direction of the underlying polymer backbone, and allow us to accurately determine the relative angle between the sliding direction and the backbone direction. Herein this angle will be referred to as the "domain

orientation", where ±90° (0°) represents scanning perpendicular (parallel) to the backbone orientation.

Friction was measured as a function of angle for 14 separate domains with a range of orientations (Fig. 5). At least three measurements were acquired on different regions of each domain. The values plotted represent the average of the difference between trace and retrace 1 × 1 μm^2 lateral force images. Friction is lowest when sliding parallel to the backbones, and maximal when sliding perpendicular, representing an increase of ~300%. For all measurements, zero externally applied load was used. The adhesion force, determined from force-distance curves on every domain, was measured to be 35±7 nN, and had no correlation with domain orientation.

3.3 Friction Asymmetry

We also attempted to observe friction asymmetry, which could possibly be induced by the molecular tilt of the pendant methylene side chains [11]. Friction asymmetry is manifested by an offset of the friction loop from zero force [7,8,11]. However, the friction loop may be offset by instrumental artifacts such as misalignment of the deflection sensing components. If friction asymmetry is maximal for a particular domain orientation, it should be minimal for an orthogonal orientation [11]. Thus, we looked for a relative change in the center of the friction loop between neighboring domains with orthogonal orientations. As shown in Fig. 6, no effect is observed. However, there is significant spatial fluctuation in the lateral force signal. This fluctuation is an inherent property of the film, due to the striations described in Fig. 4, and obscures the observation of friction asymmetry below 10% of the maximum friction signal.

4. Discussion

4.1 Friction Anisotropy

The observed friction anisotropy is clearly associated with the polymer backbone direction, as independently verified with topographic AFM images and polarized fluorescence microscopy. The angular dependence of the friction force F_f (Fig. 5) can be simply modeled by the following equation:

$$F_f = F_1 + F_2 \cdot |\sin\theta| \qquad (1)$$

where θ represents the domain orientation. F_1 represents the angle-independent contribution to friction and can be thought of as an intrinsic friction force between the film and the tip. F_2 represents an additional contribution to friction that arises when there is a component of sliding motion perpendicular to the polymer backbone direction. The origin of this force is discussed below. The absolute value is used to ensure that this contribution is positive. Equation (1) provides a consistent fit to the data as shown in Fig. 5, giving $F_1 = 77$ mV and $F_2 = 144$ mV. Thus, according to the fit, the total friction anisotropy is $F_{max} = \frac{F_1 + F_2}{F_1} = 2.9$.

We propose that this effect is due to anisotropic lateral film stiffness caused by anisotropic packing and/or ordering of the alkyl side chains as well as the anisotropic stiffness of the polymer backbone itself. Along the backbone direction, the extended conjugated polymer bonds provides a rigid link between alkyl chains, and imposes a regular spacing of 4.9 Å (Fig. 1) [15]. This spacing simultaneously satisfies the bond lengths of the polymer backbone as well as the equilibrium van der Waals' spacing of the alkyl chains with an appropriate tilt angle (Fig. 1). Indeed, we observe regular stick-slip friction with ~5 Å periodicity along the backbone direction for these films. However, the spacing between alkyl chains linked to *neighboring* backbones is determined by weaker interchain van der Waals' forces and possibly by the spacing of the head groups which are bonded to the mica substrate. The head groups are not necessarily uniformly spaced in the direction perpendicular to the backbones and may be influenced by the substrate lattice. In other words, the lack of covalent bonding between neighboring polymer chains allows some freedom in their spacing. Indeed, Lio *et al.* observed such anisotropic spacing in atomic

lattice-resolved images of a similar polydiacetylene thin film [33,20]. In fact, variations in film density could explain the film height contrast observed in Fig. 4(a). Both the tilt angle and gauche defect population of films of alkyl chains are affected by packing density [34-36]. Regions with different density are therefore likely to exhibit height variations due to different tilt angles of the alkyl chains and/or increased number of gauche defects. However, as seen in Fig. 4, friction is not correlated with the local height of these individual regions. Rather, the reduced packing density and lack of covalent bonding perpendicular to the backbone direction leads to higher friction when sliding along this direction as discussed below.

Several observations with AFM have indicated that lower packing density and/or increased disorder of monolayer alkane films leads to increased friction [37-40]. It is proposed that a lower packing density provides increased freedom to displace molecules during sliding (low lateral stiffness), possibly by increasing the contact area and also providing more channels for energy dissipation. For our system, we propose that there is high lateral stiffness when sliding the tip along the backbone direction, as the molecules are densely packed and rigidly linked in this direction and have little freedom to be displaced. Thus a minimum friction force is expected. However, any component of motion perpendicular to the chains could lead to increased molecular displacement and correspondingly increased friction. According to this model, the increase in friction should be proportional to the vector component of the sliding direction perpendicular to the backbone direction. This is indeed the model proposed in Equation (1), and is clearly consistent with the data in Fig. 5. Further measurements, specifically lateral stiffness measurements [41] are required to verify this hypothesis. We can only state at this point that this proposed model is consistent with both our observations and the existing examples in the literature.

4.2 Friction Asymmetry

As previously mentioned, friction asymmetry has been observed to be induced by the tilt of molecular groups from the surface normal, although it is a relatively subtle effect. Bluhm *et al.* [7,8] observed friction asymmetry with a ferroelectric material, triglycine sulfate, which corresponded to ~4% of the total friction force. Liley *et al.* [11] observed friction asymmetry of a thiolipid Langmuir-Blodgett monolayer of ~15% of the friction force. The thiolipid monolayer consists of domains with alkyl chains uniformly tilted with respect to the surface normal. The alkyl chains, with which the tip interacts, are linked to each other by a complex head group that is bound to the substrate. Asymmetry was observed when scanning the AFM tip back and forth along the tilt direction of the alkyl chains. We believe that the alkyl chains in our monolayer film are tilted with respect to the surface normal, as indicated by film height measurements, and consistent with other structural studies of polydiacetylene thin films[20,42]. This tilt could perhaps cause friction asymmetry, but spatial fluctuations of the friction force, as discussed above, obscure this effect if it is present. It is not known if friction asymmetry is a universal effect; despite a vast number of AFM studies of ordered alkanethiol monolayers[1], whose alkyl chains are uniformly tilted at ~30° with respect to the surface normal, no friction asymmetry has yet been reported.

5. Conclusion

Monolayer films of PCEA exhibit strong friction anisotropy of ~300%. This strong friction anisotropy may allow this system to be used for nanofabrication, as the film provides a substrate with a single preferred sliding direction within a given domain, and the direction can be remotely determined using optical microscopy. Friction is highest when scanning perpendicular to the polymer backbone direction. We propose that this effect results from anisotropic film stiffness. Further measurements of the directional dependence of film stiffness are needed to verify this hypothesis.

Acknowledgements

We acknowledge useful discussions with M. Crawford, D.H. Charych, U. Jonas, J.E. Houston and T. Michalske. R.W.C. acknowledges the support of the Natural Sciences and Engineering Research Council of Canada. Sandia is a multiprogram laboratory operated by Sandia Corporation, a Lockheed Martin Company, for the United States Department of Energy under Contract DE-AC04-94AL85000.

References

[1] R.W. Carpick and M. Salmeron, Chem. Rev. 97 (1997) 1163.

[2] R.W. Carpick, N. Agraït, D.F. Ogletree and M. Salmeron, J. Vac. Sci. Technol. B 14 (1996) 1289.

[3] H. Yoshizawa, Y.-L. Chen and J. Israelachvili, Wear 168 (1993) 161.

[4] T. Bouhacina, J.P. Aime, S. Gauthier, D. Michel and V. Heroguez, Phys. Rev. B 56 (1997) 7694.

[5] M. Hirano, K. Shinjo, R. Kaneko and Y. Murata, Phys. Rev. Lett. 67 (1991) 2642.

[6] R.M. Overney, H. Takano, M. Fujihira, W. Paulus and H. Ringsdorf, Phys. Rev. Lett. 72 (1994) 3546.

[7] H. Bluhm, U.D. Schwarz, K.P. Meyer and R. Wiesendanger, Appl. Phys. A 61 (1995) 525.

[8] U.D. Schwarz, H. Bluhm, H. Hölscher, W. Allers and R. Wiesendanger, in: *Physics of Sliding Friction* edited by B. N. J. Persson and E. Tosatti, (Kluwer Academic Publishers, 1996), pp. 369UCB Physics QC197 .A27 1995

UCD Phys Sci QC197.A27 1996 .

[9] P.E. Sheehan and C.M. Lieber, Science 272 (1996) 1158.

[10] U. Gehlert, J.Y. Fang and C.M. Knobler, Journal of Physical Chemistry B 102 (1998) 2614.

[11] M. Liley, D. Gourdon, D. Stamou, U. Meseth, T.M. Fischer, C. Lautz, H. Stahlberg, H. Vogel, N.A. Burnham and C. Duschl, Science 280 (1998) 273.

[12] R. Pearce and G.J. Vancso, Polymer 39 (1998) 6743.

[13] A. Artsyukhovich, L.D. Broekman and M. Salmeron, Langmuir 15 (1999) 2217.

[14] D. Bloor and R.R. Chance, in: *Polydiacetylenes: Synthesis, Structure, and Electronic Properties*, edited by D. Bloor and R.R. Chance, Martinus Nijhoff, Dordrecht, 1985.

[15] A. Ulman, in: *Introduction to Ultrathin Organic Films from Langmuir-Blodgett to Self-Assembly* (Academic Press, 1991), pp. 182-191 and references therein .

[16] D.N. Batchelder, S.D. Evans, T.L. Freeman, L. Haussling, H. Ringsdorf and H. Wolf, J. Am. Chem. Soc. 116 (1994) 1050.

[17] T. Kim and R.M. Crooks, Tetrahedron Letters 35 (1994) 9501.

[18] M.D. Mowery and C.E. Evans, Tetrahedron Letters 38 (1997) 11.

[19] M. Wenzel and G.H. Atkinson, J. Am. Chem. Soc. 111 (1989) 6123.

[20] A. Lio, A. Reichert, D.J. Ahn, J.O. Nagy, M. Salmeron and D.H. Charych, Langmuir 13 (1997) 6524.

[21] H. Muller and C.J. Eckhardt, Mol. Cryst. Liq. Cryst. 45 (1978) 313.

[22] Y. Tomioka, N. Tanaka and S. Imazeki, J. Chem. Phys. 91 (1989) 5694.

[23] R.A. Nallicheri and M.F. Rubner, Macromolecules 24 (1991) 517.

[24] D.H. Charych, J.O. Nagy, W. Spevak and M.D. Bednarski, Science 261 (1993) 585.

[25] A. Reichert, J.O. Nagy, W. Spevak and D. Charych, J. Am. Chem. Soc. 117 (1995) 829.

[26] D. Charych, Q. Cheng, A. Reichert, G. Kuziemko, M. Stroh, J.O. Nagy, W. Spevak and R.C. Stevens, Chemistry & Biology 3 (1996) 113.

[27] R.W. Carpick, D.Y. Sasaki and A.R. Burns, in preparation (1999) .

[28] D.Y. Sasaki, R.W. Carpick and A.R. Burns, in preparation (1999) .

[29] D.F. Ogletree, R.W. Carpick and M. Salmeron, Rev. Sci. Instrum. 67 (1996) 3298.

[30] R.R. Chance, G.N. Patel and J.D. Witt, J. Chem. Phys. 71 (1979) 206.

[31] M.H.P. Moers, H.E. Gaub and N.F. Vanhulst, Langmuir 10 (1994) 2774.

[32] S. Yamada and Y. Shimoyama, Jpn. J. Appl. Phys. 1, Regul. Pap. 35 (1996) 4480.

[33] A. Lio, A. Reichert, J.O. Nagy, M. Salmeron and D.H. Charych, J. Vac. Sci. Technol. B 14 (1996) 1481.

[34] M.D. Porter, T.B. Bright, D.L. Allara and C.E.D. Chidsey, J. Am. Chem. Soc. 109 (1987) 3559.

[35] M.A. Bryant and J.E. Pemberton, J. Am. Chem. Soc. 113 (1991) 8284.

[36] P. Fenter, P. Eisenberger and K.S. Liang, Phys. Rev. Lett. 70 (1993) 2447.

[37] A. Lio, D.H. Charych and M. Salmeron, Journal of Physical Chemistry B 101 (1997) 3800.

[38] M.T. McDermott, J.-B.D. Green and M.D. Porter, Langmuir 13 (1997) 2505.

[39] J.D. Kiely, J.E. Houston, J.A. Mulder, R.P. Hsung and X.Y. Zhu, Trib. Lett. this volume (1999) .

[40] J.D. Kiely, N.D. Shinn and J.E. Houston, Langmuir in preparation (1999) .

[41] R.W. Carpick, D.F. Ogletree and M. Salmeron, Appl. Phys. Lett. 70 (1997) 1548.

[42] M.D. Mowery, H. Menzel, M. Cai and C.E. Evans, Langmuir 14 (1998) 5594.

Figure Captions

Fig. 1. (a) PCEA monomer and (b) polymer showing the ethanol-amine head group bound to the substrate. Dotted lines represent possible hydrogen bonding interactions. The polymer backbone repeat unit of polydiacetylene is expected to be 4.9 Å.

Fig. 2. 170 × 100 μm^2 polarized fluorescence microscopy images. The arrows on the left represent the polarization direction, which is roughly (a) –45°, (b) 0° and (c) +45 °. The polymer backbone direction of three domains is indicated by the other arrows. High fluorescence occurs when the polarization is aligned with backbone direction, and is dramatically reduced when the polarization is nearly orthogonal to the backbone direction (white arrows).

Fig. 3. 50 × 50 μm^2 AFM images of the PCEA monolayer. (a) Topography. (b) Friction. The topography is flat to within 2-3 Å, with the exception of some material piled up at a fraction of the domain boundaries. The friction image reveals the different domains. The white arrows indicate the domain orientation, determined from higher resolution images like those in Fig. 4.

Fig. 4. 500 × 500 nm^2 images within a single domain. (a) Topography. (b) Friction. Linear striations are observed, which reveal the backbone orientation. The topography image displays ~2 Å height variations between different striations. There is some variation in the friction signal as well, but the friction force is uniform to within ~10%.

Fig. 5. Friction force (raw signal units) *vs.* angle. 0° indicates sliding parallel to the backbone direction. Friction is calculated by taking the difference between trace and retrace images (1 × 1 μm^2, 256 × 256 pixels) on single domains. The edges of the image were excluded so as to only

sample the sliding portion of the measurement. Each measurement represents the average value of approximately 40,000 pixels. The standard deviation is used for the friction error bars. The solid line represents the fit of Eq. (1) to the data.

Fig. 6. Lateral force trace, retrace, and the sum of the trace and retrace signals over two orthogonal domains. Although the loop width (*i.e.* friction force) varies greatly between the two domains, the sum is nearly constant. This indicates that there is no observable friction asymmetry on either of these domains. However, there is a ~10% spatial variation in the friction signals, rendering the observation of a small asymmetry effect difficult.

fig. 1

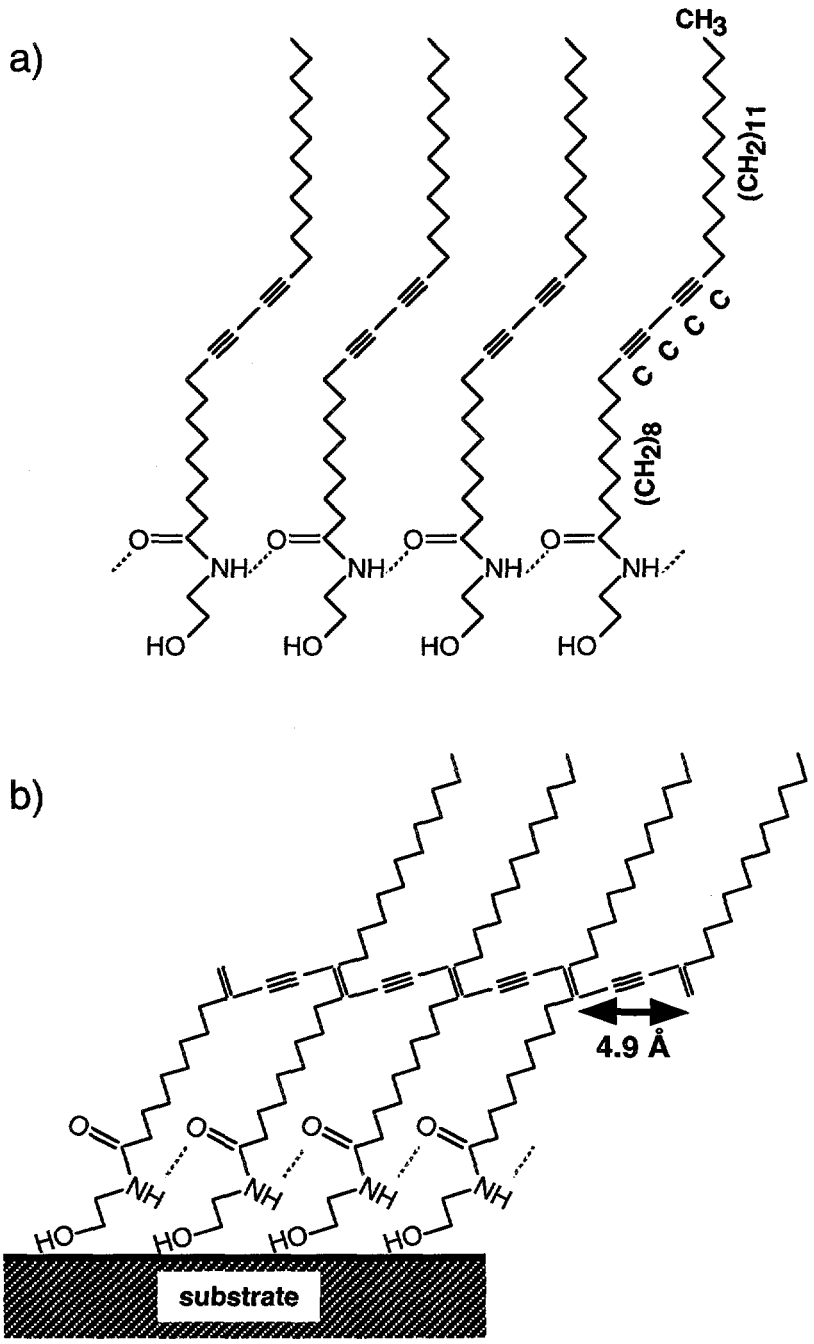

fig. 2

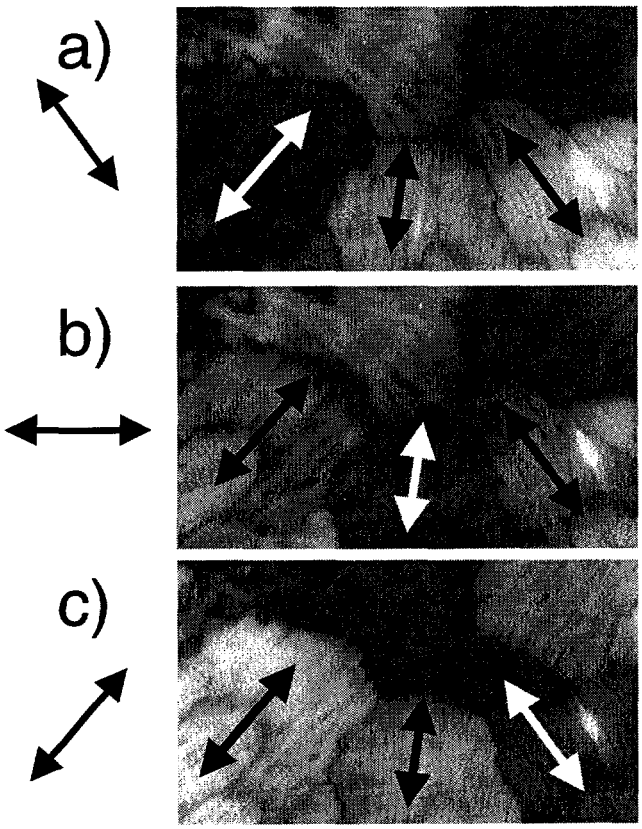

fig. 3

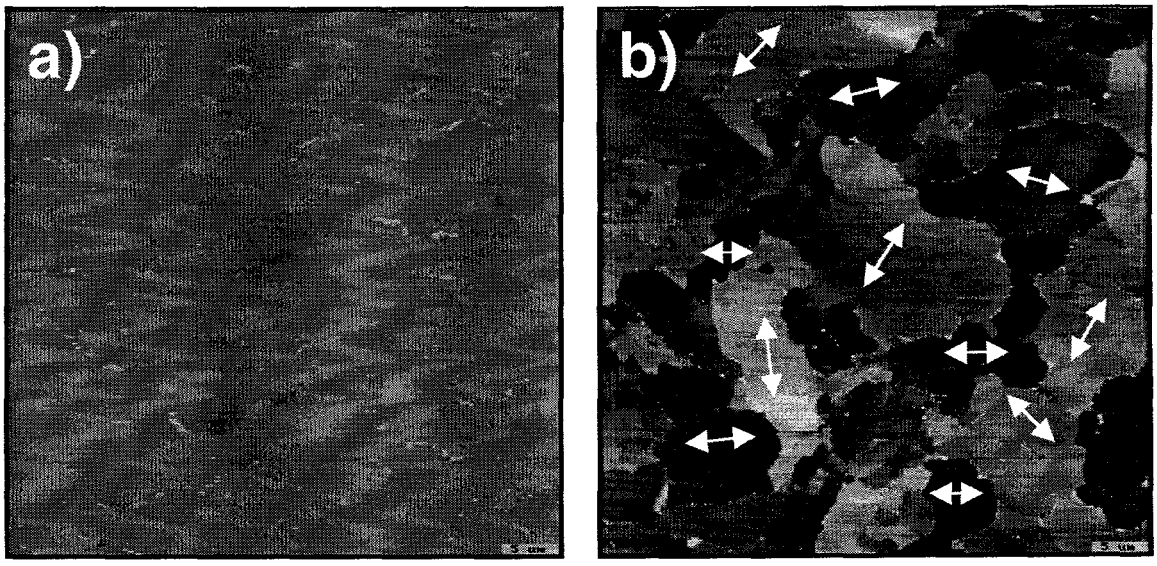

fig. 4

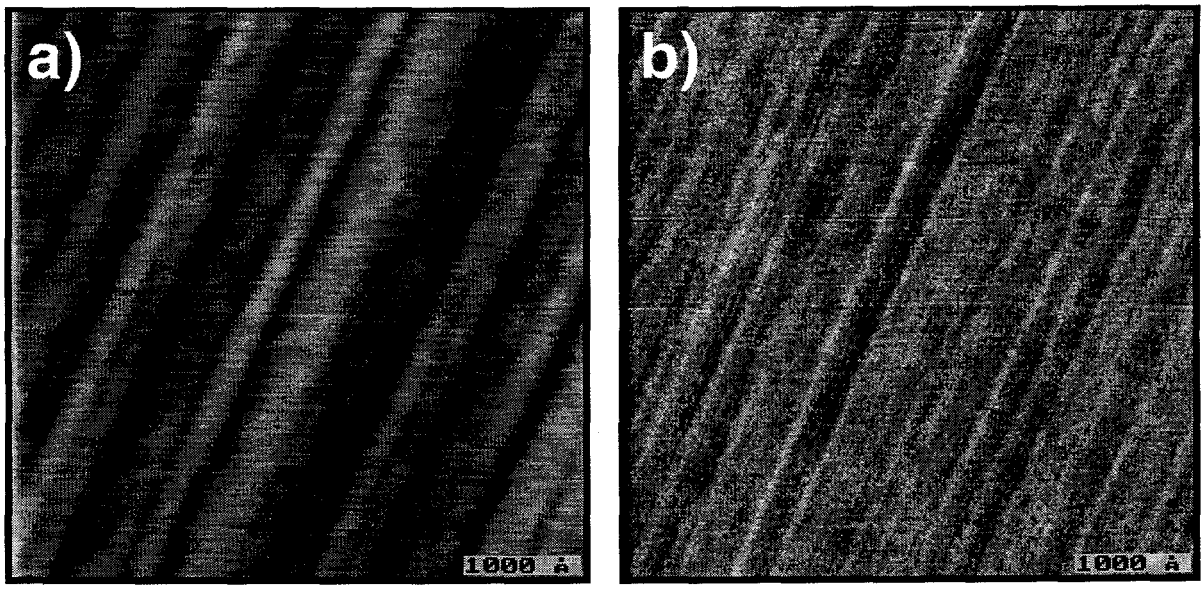

fig. 5

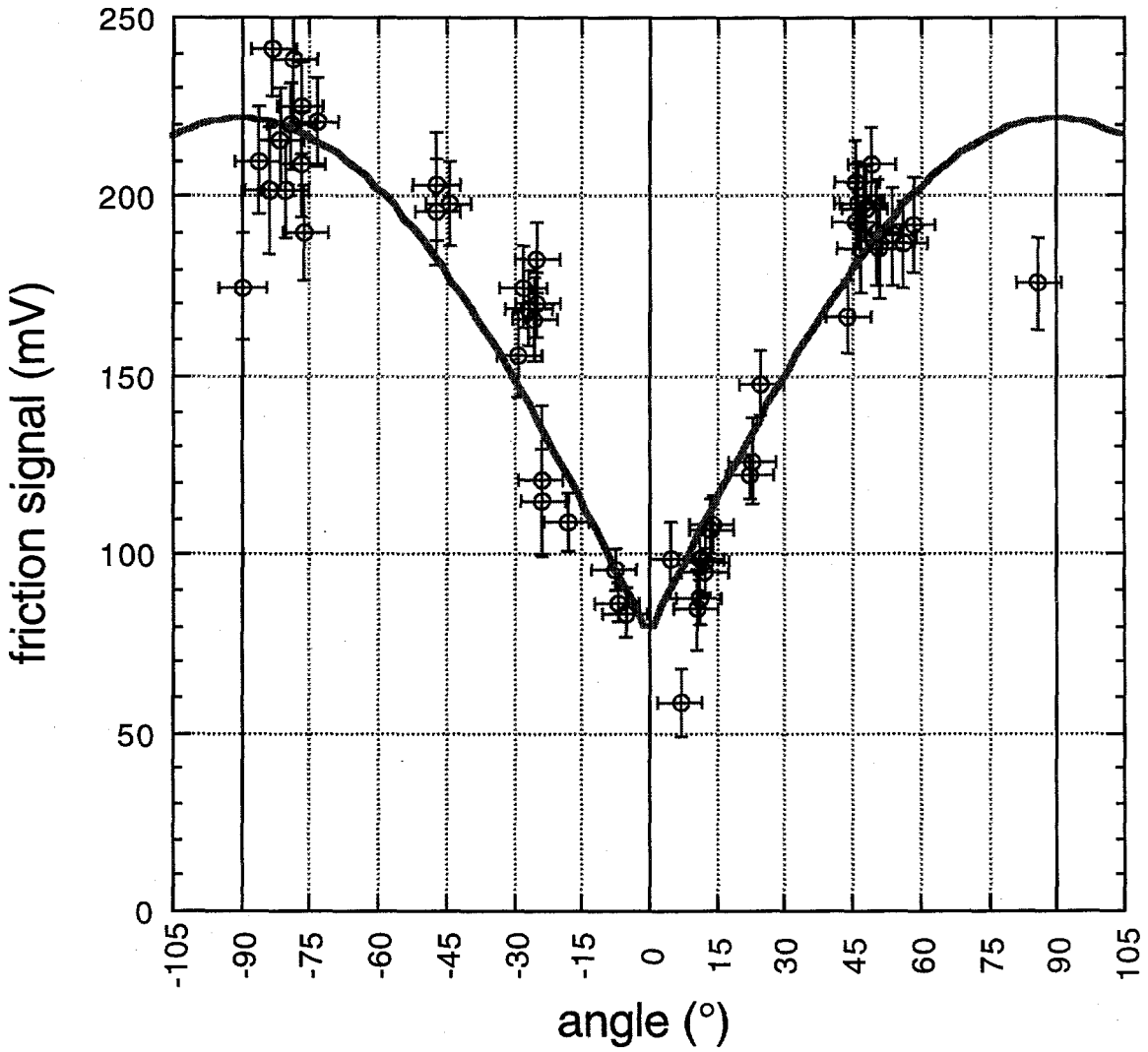
friction signal (mV)
250
200
150
100
50
0
-105
-90
-75
-60
-45
-30
-15
0
15
30
45
60
75
90
105
angle (°)

fig. 6

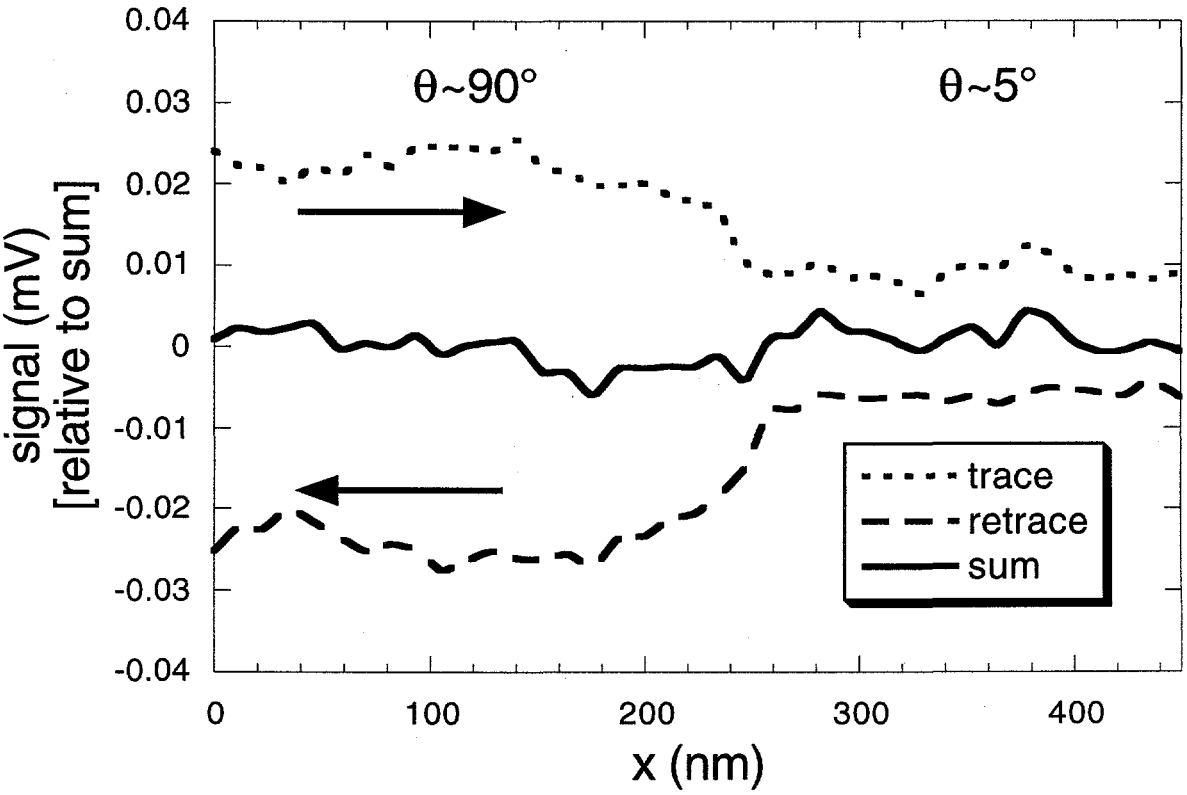
0.04
0.03
0.02
0.01
0
-0.01
-0.02
-0.03
-0.04
signal (mV)
[relative to sum]
θ~90°
θ~5°
trace
retrace
sum
0
100
200
300
400
x (nm)